Hindawi
Journal of Nanomaterials
Volume 2019, Article ID 2182471, 9 pages
https://doi.org/10.1155/2019/2182471

Research Article

Immobilization of Protein A on Monodisperse Magnetic Nanoparticles for Biomedical Applications

Bui Trung Thanh,[1,2] Nguyen Van Sau,[3] Heongkyu Ju,[4] Mohammed J. K. Bashir,[5] Hieng Kiat Jun,[6] Thang Bach Phan,[7] Quang Minh Ngo,[8,9,10] Ngoc Quyen Tran,[11,12] Tran Hoang Hai,[13] Pham Hung Van,[14] and Tan Tai Nguyen[15]

[1]*Department of Physics, University of Medicine and Pharmacy at Ho Chi Minh City 70000, Vietnam*
[2]*Solid State Physics Department, University of Science, Vietnam National University, Ho Chi Minh City 70000, Vietnam*
[3]*School of Basic Science, Tra Vinh University, Tra Vinh City 87000, Vietnam*
[4]*Department of Nano-Physics, Gachon University, 1342 Seongnam-daero, Sujeong-gu, Seongnam-si, Gyeonggi-do 13120, Republic of Korea*
[5]*Faculty of Engineering and Green Technology (FEGT), Universiti Tunku Abdul Rahman, 31900 Kampar, Perak, Malaysia*
[6]*Department of Mechanical and Material Engineering, Lee Kong Chian Faculty of Engineering and Science, Universiti Tunku Abdul Rahman, Sungai Long Campus, Bandar Sg. Long, 43000 Kajang, Malaysia*
[7]*Center for Innovative Materials and Architectures, Vietnam National University, Ho Chi Minh City, Vietnam*
[8]*Institute of Materials Science, Vietnam Academy of Science and Technology, 18 Hoang Quoc Viet, Cau Giay, Hanoi, Vietnam*
[9]*Graduate University of Science and Technology, Vietnam Academy of Science and Technology, 18 Hoang Quoc Viet, Cau Giay, Hanoi, Vietnam*
[10]*University of Science and Technology of Hanoi, Vietnam Academy of Science and Technology, 18 Hoang Quoc Viet, Cau Giay, Hanoi, Vietnam*
[11]*Graduate University of Science and Technology, Vietnam Academy of Science and Technology, Ho Chi Minh City 70000, Vietnam*
[12]*Institute of Applied Materials Science, Vietnam Academy of Science and Technology, Ho Chi Minh City 70000, Vietnam*
[13]*Institute of Physics, Ho Chi Minh City 70000, Vietnam*
[14]*Department of Physics, University of Medicine and Pharmacy, Ho Chi Minh City 70000, Vietnam*
[15]*Department of Materials Science, School of Applied Chemistry, Tra Vinh University, Tra Vinh City 87000, Vietnam*

Correspondence should be addressed to Tan Tai Nguyen; nttai60@gmail.com

Received 11 October 2018; Revised 30 January 2019; Accepted 12 February 2019; Published 24 March 2019

Academic Editor: Jean M. Greneche

We presented synthesis and physical characterization of iron oxide magnetic nanoparticles (Fe_3O_4) for biomedical applications in the size range of 10-30 nm. Magnetic nanoparticles were synthesized by the coprecipitation method, and the particles' size was controlled by two different injection methods of sodium hydroxide (NaOH). The synthesized magnetic nanoparticles were then modified by using series of linkers including tetraethyl orthosilicate (TEOS), 3-aminopropyltriethoxysilane (APTES), and glutaraldehyde (GA) to generate the structure of $Fe_3O_4/SiO_2/NH_2/CHO$, which can be used for immobilization of protein A. Additionally, we used transmission electron microscopy (TEM), X-ray powder diffraction (XRD), vibrating-sample magnetometry (VSM), and Fourier-transform infrared spectroscopy (FTIR), for characterization of properties and structure of the nanoparticles. An immobilization of protein A on magnetic nanoparticles was studied with a UV-Vis spectrum (UV-Vis) and fluorescence electron microscopy and Bradford method. Results showed that an XRD spectrum with a peak at (311) corresponded to the standard peak of magnetic nanoparticles. In addition, the magnetic nanoparticles with $d \geq 30$ nm have higher saturation magnetizations in comparison with the smaller ones with $d \leq 10$ nm. However, the smaller magnetic nanoparticles offered higher efficiency for binding of protein A, due to the high surface/volume ratio. These particles with functional groups on their surface are promising candidates for biomedical applications, e.g., drug delivery, controlled drug release, or disease diagnosis in point-of-care test.

1. Introduction

Nowadays, there are various sorts of virus and bacterial pathogens that cause disease *in vivo* and human death [1–3]. Infectious elements cause various cancers or tumors are basically required to be detected to prevent the infection and the transmission. The available detection techniques include the traditional methods of treating diseases such as enzyme-linked immunosorbent assay (ELISA) based on antigen-antibody interaction [4–6] and polymerase chain reaction (PCR) which amplified DNA molecules through temperature-dependent cyclic steps [7–10]. According to improved research direction in nanomedicine, they require integration of detection and diagnosis as well as therapy with modern molecular imaging and living-cell detection.

In the past few decades, nanotechnology has been considered as an important advancement in science and technology. It is related to the production of materials at the nanometer scale. There has been a large research interest in nanoscale materials that is due to their unique properties such as high surface area, large number of binding sites on their surface, high surface reactivity, and strong absorption activity [11–14]. Those characteristics offer novel application in biomedicine. Nowadays, technologies have been developed for detection and treatment of various diseases such as nanodispensing systems using carbon nanotubes (CNTs) for chemotherapy [15, 16], drug delivery system using silica nanoparticles (SiO_2) with attached fluorescent dye molecules [17–20], using silver (Ag) nanoparticles for antibacterial property against clinically isolated multidrug-resistant microorganisms [21, 22], and biosensor utilizing gold (Au) nanoparticles for DNA detection [23, 24]. However, those methods have inherent drawbacks due to the lack of carrier properties. For example, those particles cannot be controlled to deliver drug into the target organisms.

In recent years, a great deal of efforts has been focused on the development of nanocarriers for diagnosis and treatment of diseases. One of the nanocarriers is magnetic nanoparticles under control of an external magnetic field. Magnetic nanoparticles are superparamagnetic materials with high saturation magnetization, nontoxic, and highly biocompatible which have great potential for biomedical applications such as efficient bioseparation, sensitive biosensing, and specific drug delivery as well as magnetic resonance imaging (MRI) contrast enhancement [25, 26]. Various sizes of superparamagnetic nanoparticles offer potential application in biomedicine with various elements including cell (around 100 μm), proteins (around 10 nm), and virus (around 100 nm) [27–29]. However, the change in size of magnetic nanoparticles is associated with the change in saturation moment, which is an important property to demonstrate the resonant responsibility to an external magnetic field of the particles. Additionally, the promising biomedical applications of magnetic nanoparticles basically require the particles to monodisperse. So the magnetic nanoparticles are required to be covered by nonmagnetic materials to prevent oxidation and agglomeration. Consequently, each nanoparticle has identical chemical and physical properties for controlled bioelimination and biodistribution [30–34].

Recently, extensive researches have shown that protein A is one of the promising biochemical linkers because of its ability to bind with immunoglobulins, fibrinogen, and C-reactive protein (CRP) [35]. This property led us to attempt to detect target proteins for disease diagnosis.

In this work, we demonstrated superparamagnetic nanoparticles for immunoassay with its modified surface ($Fe_3O_4/SiO_2/NH_2/CHO$) for immobilization of protein A. The heterogeneous layers were coated for a wide dynamic range of detection and high specificity of the particle surface. We coated silica layer (SiO_2) on the magnetic nanoparticle surface for a subsequent self-assembled monolayer of aminopropyltriethoxysilane (APTES) and glutaraldehyde (GA) for subsequent absorption of protein A, which could capture target molecules specifically. We characterized successive immobilization of each layer of SiO_2, NH_2, CHO, and protein A in a quantitative manner. The absorption efficiency of protein A is 82.35% and 52.94% for the size of the synthesized magnetic nanoparticles of 10 nm and 30 nm, respectively. This led us to believe that the synthesized magnetic nanoparticles could find potential applications for disease diagnosis and disease treatment.

2. Materials and Methods

2.1. Agents. Iron(II) chloride tetrahydrate ($FeCl_2{\cdot}4H_2O$) (≥99%), iron(III) chloride hexahydrate ($FeCl_3{\cdot}6H_2O$) (≥99%), ammonium hydroxide ($NH_3{\cdot}H_2O$) (≥99%), sodium hydroxide (NaOH) (≥98%), ethanol (C_2H_5OH) (99%), and phosphate-buffered saline (PBS, pH 7.4) were purchased from Merck. Glutaraldehyde (GA), 3-aminopropyltriethoxysilane (APTES), biotin ($C_{10}H_{16}N_2O_3S$) (≥99%), biotin-fluorescence isothiocyanate (biotin-FITC, $C_{33}H_{32}N_4O_8S$), and tetraethyl orthosilicate (TEOS, $Si(OC_2H_5)_4$) (≥99%) were bought from Sigma-Aldrich.

2.2. Fabrication of Magnetic Nanoparticles. Magnetic nanoparticles were synthesized based on the coprecipitation method, and its size could be controlled by change in pH of solutions, types of base, ionic concentration, mole concentration ratio between Fe^{2+} and Fe^{3+}, and reaction temperature [36, 37]. The optimized amount between Fe^{2+} and Fe^{3+} was a mole concentration ratio of 1 : 2 [36]. In this work, we used 4.3 g of $FeCl_3.6H_2O$ mixed with 1.6 g of $FeCl_2.4H_2O$ and then diluted with 120 mL of distilled water (DI). After that, this solution was separated into two parts and stored under nitrogen gas condition. Additionally, two parts of mixing solution were vigorously stirred with a speed of 800 cycles/min at a temperature of 80°C within 15 min. In this work, we controlled the size of magnetic nanoparticles by change in injection methods of sodium hydroxide solution [37]. 2 mL of 2 M sodium hydroxide was immediately injected in the first mixing solution while a similar amount of sodium hydroxide was dropped into the second one. Both parts were continuously stirred within 45 min and then cooled down to room temperature. This synthesized nanoparticles (Fe_3O_4) were washed by DI water (three times at least) via magnetic decantation and then dried in vacuum at 40°C.

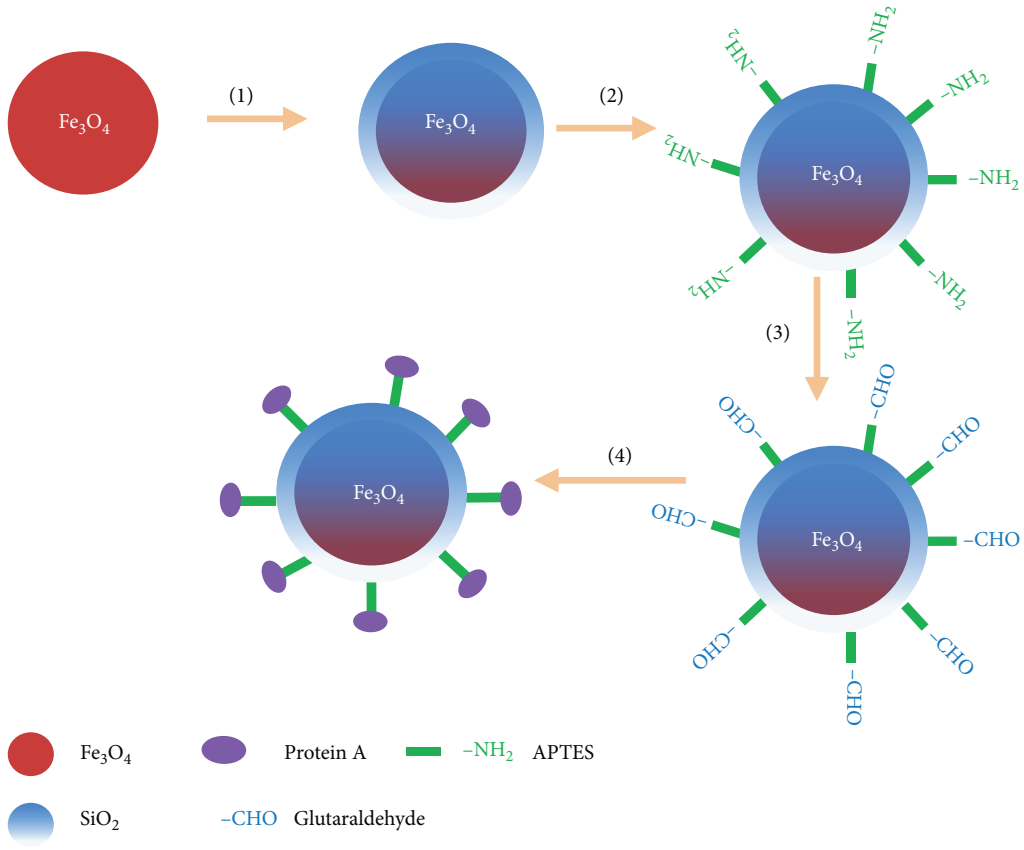

Figure 1: Procedures for immobilization of protein A on the synthesized superparamagnetic nanoparticles. Notes: (1) SiO_2 covering; (2) self-assembled monolayer of APTES; (3) self-assembled monolayer of glutaraldehyde; (4) immobilization of protein A.

2.3. Immobilization of Protein A on Synthesized Nanoparticles. The surface of Fe_3O_4 nanoparticles was then modified with a functional group for immobilization of protein A. For biomedical application, Fe_3O_4 nanoparticles should be monodisperse by covering of nonmagnetic materials [38]. As shown in Figure 1, Fe_3O_4 nanoparticles were covered by the silica layer (SiO_2) based on the Stober method [37]. In this case, 200 mg of Fe_3O_4 nanoparticles was diluted into 50 mL of mixing solution including ethanol and DI water with a volume ratio of 3 : 2. After that, TEOS at 2 mL and NH_3(l) were subsequently injected to the suspension and stirred at a speed of 100 cycles/minute for 24 h with temperature of 40°C under nitrogen gas. Then, this solution was stirred by using an ultrasonic machine for 30 min. Finally, we obtained modified magnetic nanoparticles with a core-shell structure of Fe_3O_4/SiO_2 as shown in Figure 1. The silica-coated particles were then washed with DI water to remove the excess solution while the magnetic nanoparticles were retained via magnetic decantation. The silica-coated magnetic nanoparticles were dried in vacuum at 40°C.

To form an amine group on the particle surface, Fe_3O_4/SiO_2 nanoparticles were diluted into a solution of ethanol mixed with DI water with a volume ratio of 1 : 2. Then, 0.63 mL of APTES was subsequently injected into that solution, which was stirred in nitrogen gas medium at 40°C for 24 h [39]. Then, the modified particles ($Fe_3O_4/SiO_2/NH_2$) were washed by DI water three times and then dried in vacuum at 40°C.

For the generation of a –CHO group to immobilize protein A, $Fe_3O_4/SiO_2/NH_2$ nanoparticles were diluted with DI water and mechanically stirred at the speed of 100 cycles/min at room temperature to make dispersion of the nanoparticles. Then, 1 mL of 25% glutaraldehyde (GA) was injected into the mentioned suspension and continuously stirred for 24 h to generate the structure of $Fe_3O_4/SiO_2/NH_2/CHO$ as shown in Figure 1. The impurities on obtained nanoparticles were removed by washing with PBS three times.

For immobilization of protein A on magnetic nanoparticles, 100 mg of $Fe_3O_4/SiO_2/NH_2/CHO$ nanoparticles was mixed with 0.5 mg of protein A [40]. Then, the mixture was diluted into 15 mL of PBS for 12 h at room temperature. Then, we used a magnetic bar to collect the magnetic nanoparticles with conjugation of protein A. The nonspecific bonding of protein A was eliminated by washing with PBS three times.

3. Results and Discussion

Figure 2 shows the XRD spectra of the synthesized magnetic nanoparticles using the coprecipitation method. In this method, we controlled the size of particles by change in the injection method of the base. Figure 2(a) corresponds to the patterns of magnetic nanoparticles synthesized with

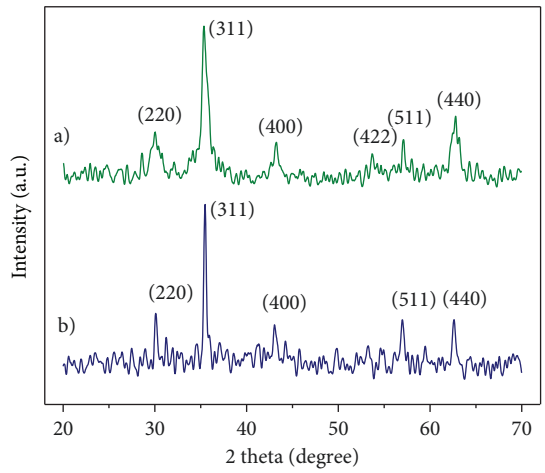

FIGURE 2: XRD patterns of the synthesized magnetic nanoparticles with two different injection methods of sodium hydroxide: (a) immediately injection of NaOH; (b) droplet of NaOH.

immediate injection of sodium hydroxide whereas Figure 2(b) shows the patterns of the synthesized nanoparticles by a droplet of sodium hydroxide.

As shown in Figure 2, the crystalline nature of magnetic nanoparticles exhibits six distinct peaks at (220), (311), (400), (422), (511), and (440), which are consistent with the expected composition of Fe_3O_4. The position and relative intensity of diffraction peaks for both patterns (Figures 2(a) and 2(b)) are also matched with the database in JCPDS file (No. 01-075-1373) for bulk Fe_3O_4. These results indicated that the synthesized particles were mainly consisted of magnetite Fe_3O_4. Additionally, we also estimated the average size of the synthesized magnetic nanoparticles using the Debye-Scherrer equation below [41].

$$D_p = \frac{k\lambda}{\chi \cos\theta}, \quad (1)$$

where D_p is the average crystallite size of the synthesized Fe_3O_4, k is the Scherrer constant (0.8-1.39), λ is the wavelength of radiation; χ is the full width at half maximum (FWHM), and θ is the position of the maximum diffraction. We used the diffraction peak at (311) for estimation because of the high signal-to-noise ratio. The size of Fe_3O_4 particles was estimated around 10 nm and 30 nm corresponding to the synthesis with immediate injection of NaOH and a droplet of NaOH, respectively. The difference in the size of Fe_3O_4 nanoparticles (Fe_3O_4NPs) was due to the balance between the speed of sprout production and speed of crystal growth. When the speed of sprout production is faster than that of crystal growth, the particles will have the smaller size. This case was corresponding to immediate injection of NaOH into an aqueous mixture of ferric and ferrous salts which resulted in a smaller size (around 10 nm) of nanoparticles (Figure 2(a)). In the other case, the size of particles was large (around 30 nm) due to the droplet of NaOH making reduction in the speed of sprout production.

To double-check the size of the synthesized magnetic nanoparticles by XRD patterns, we conducted a TEM analysis of Fe_3O_4 nanoparticles. Figures 3(a) and 3(c) show the TEM images of the synthesized magnetic nanoparticles with two different injection methods of NaOH as we mentioned above. It was also worth noting that the similar sizes of Fe_3O_4NPs were observed in comparison with the XRD analysis using the Debye-Scherrer equation. Moreover, it was clearly shown that Fe_3O_4NPs were monodisperse and has a spherical shape, leading to offer advanced applications in biomedicine.

Additionally, Fe_3O_4NPs were then coated with a thin silica layer (2-3 nm) using the Stober method as shown in Figures 3(c) and 3(d). Note that there are a lot of factors that affect silica-coated Fe_3O_4NP size, e.g., temperature, pH, type of alcohol, amount of TEOS added, and amount of catalyst used during the process. In this work, we used ammonia to promote the condensation of TEOS. The outer silica surface of silica-coated Fe_3O_4NPs is desirable not only because it prevents agglomeration and oxidation of Fe_3O_4NPs but also because it has extensive hydroxide groups on the surface, which can be functionalized to generate various chemical linkers on its surface. Additionally, the silica layer can also offer better protection against toxicity in biological applications.

The major hysteresis loop of uncoated and SiO_2-coated Fe_3O_4NPs (primary Fe_3O_4NPs sizes of 10 nm and 30 nm) was measured by the VSM at room temperature. As shown in Figure 4, the coercivities of each sample are 63 emu/g for uncoated Fe_3O_4NPs (10 nm), 48 emu/g for SiO_2-coated Fe_3O_4NPs (10 nm), 85 emu/g for uncoated Fe_3O_4NPs (30 nm), and 76 emu/g for SiO_2-coated Fe_3O_4NPs (10 nm). Results showed that the coercivity of the SiO_2-coated Fe_3O_4NPs is lower than that of the uncoated ones and the smaller nanoparticles' size has less magnetization in comparison with the larger ones. It is well-known that the magnetic behavior of magnetite nanoparticles depends on their dipole-dipole interactions, which is strongly affected by the distance between particles. This means that the change in interparticle interactions can be used to control an agglomeration. In this work, the SiO_2 layer surrounding the Fe_3O_4NPs acts as an insulating layer to lock electron transfer, causes an increase in distance between the nanoparticles, and also prevents their agglomeration. Thus, the SiO_2-coated Fe_3O_4NPs shows a decrease in coercivity. Furthermore, magnetization of the synthesized nanoparticles is larger than that of magnetic nanoparticles as reported in the literature [42] and is comparable with the results obtained in the literatures [43, 44].

For surface functionalization of the synthesized magnetic nanoparticles, APTES was used to generate an amine group on the SiO_2 layer forming the structure of $Fe_3O_4/SiO_2/NH_2$. As shown in Figure 5, FTIR results displayed the spectra of Fe_3O_4, Fe_3O_4/SiO_2, and $Fe_3O_4/SiO_2/NH_2$ structures, which reveal the distinct peaks in the range of 3384 cm^{-1}, 1627 cm^{-1}, 1402 cm^{-1}, 1095 cm^{-1}, 956 cm^{-1}, 801 cm^{-1}, 572 cm^{-1}, and 471 cm^{-1}. The peaks at 572 cm^{-1} and 471 cm^{-1} represented the vibration of Fe-O as shown in Figure 5(a, b, and c), and those peaks also were specific ones for the Fe_3O_4 structure [39].

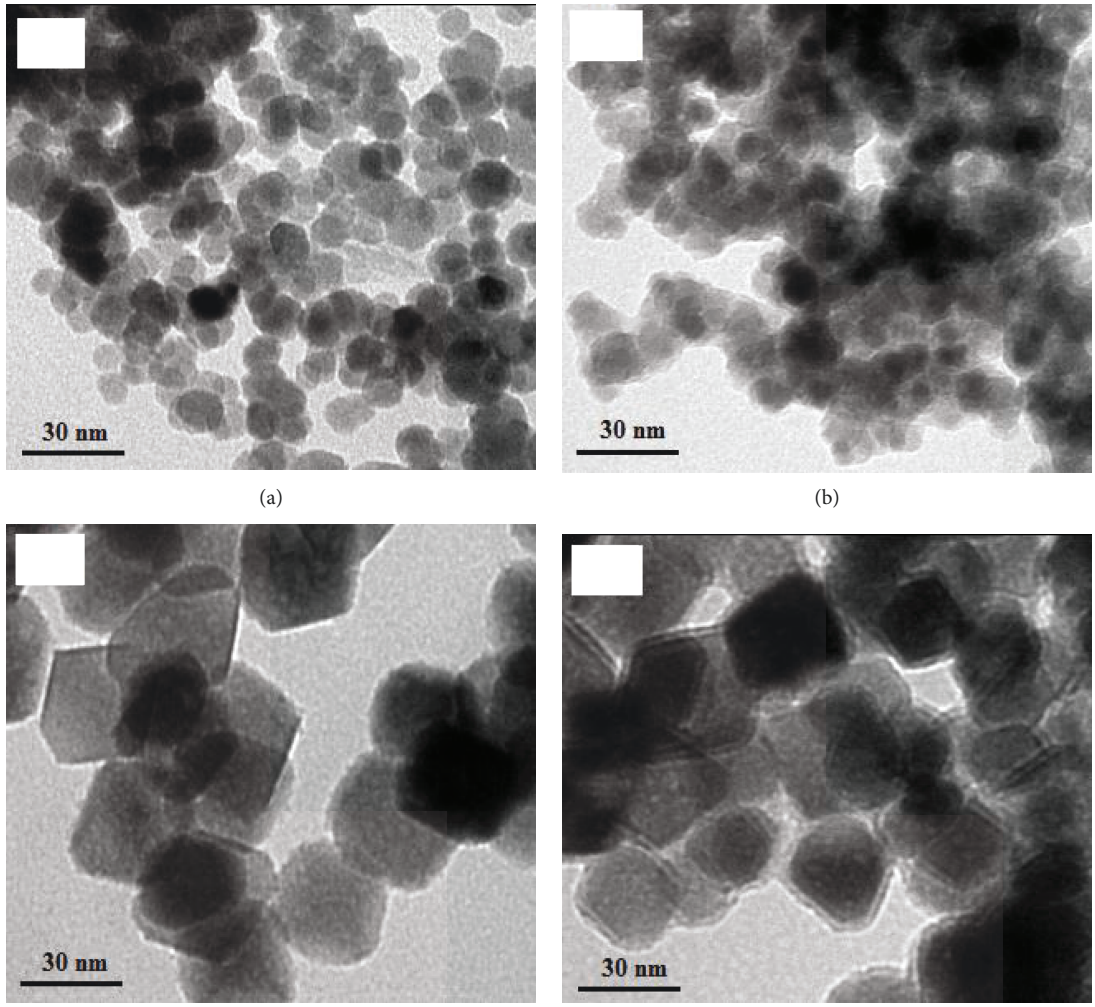

FIGURE 3: TEM images of the synthesized magnetic nanoparticles: (a) Fe_3O_4NPs of 10 nm; (b) Fe_3O_4NPs of 10 nm with a cover layer of SiO_2; (c) Fe_3O_4NPs of 30 nm; (d) Fe_3O_4NPs of 30 nm with a cover layer of SiO_2.

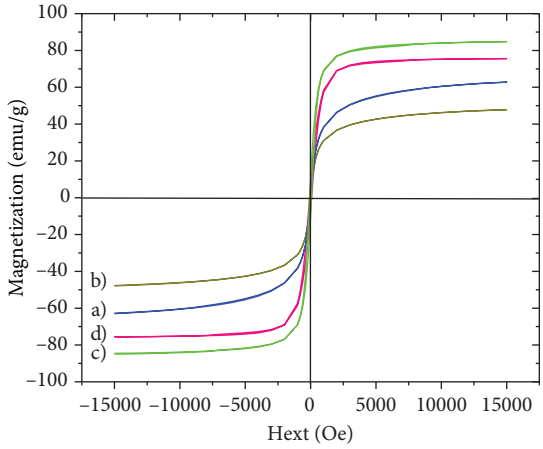

FIGURE 4: Magnetization curve of the synthesized superparamagnetic nanoparticles: (a) Fe_3O_4NPs and (b) Fe_3O_4/SiO_2 with particles' size of 10 nm; (c) Fe_3O_4NPs and (d) Fe_3O_4/SiO_2 with particles' size of 30 nm.

However, there was not a peak at 632 cm^{-1}, leading us to believe that there was not an Fe_2O_3 phase presented in the synthesized magnetic nanoparticles (Fe_3O_4) [45]. Moreover, the peak at 471 cm^{-1} was also identified as Si-O-Si bending vibrations [46], leading to enhance the intensity of this peak as shown in Figure 5(b and c). The peaks at 1095 cm^{-1} and 801 cm^{-1} also corresponded to the stretching vibrations of Si-O-Si, while the peak at 956 cm^{-1} was referred as the stretching vibrations of Si-OH [46]. This thus indicated that TEOS has covered the Fe_3O_4NPs to form an Fe_3O_4/SiO_2 structure. The bands at 3384 cm^{-1}, 1627 cm^{-1}, and 1402 cm^{-1} were found at the stretching vibrations of OH, bending vibrations of H-O-H, and bending vibrations of OH as shown in Figure 5(a, b and c), respectively [46]. In addition, the peaks at 3384 cm^{-1} and 1627 cm^{-1} were also referred as stretching vibrations of N-H and bending vibrations of amide-II [39] that caused an increase in intensity of those peaks as shown in Figure 5(c), indicating that the amine group (NH_2) has been existing on the surface of Fe_3O_4/SiO_2 to generate the structure of $Fe_3O_4/SiO_2/NH_2$. The similar spectra of FTIR

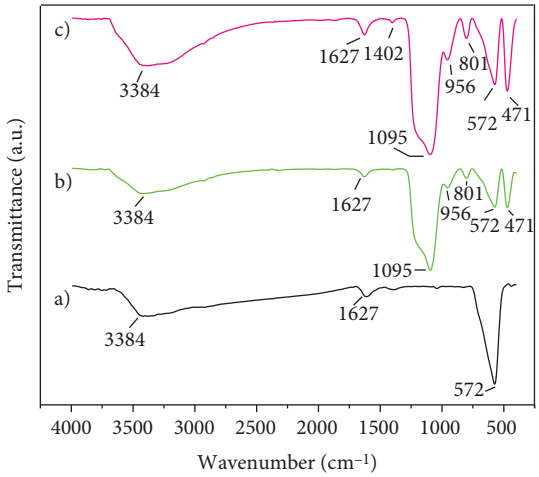

Figure 5: FTIR spectra of the superparamagnetic nanoparticles of 30 nm (a) Fe_3O_4; (b) Fe_3O_4/SiO_2; (c) $Fe_3O_4/SiO_2/NH_2$.

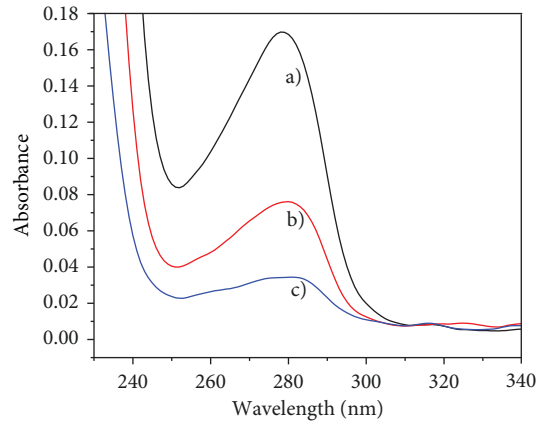

Figure 6: UV-Vis spectra of protein A concentration (a) before immobilization; after immobilization on the functional magnetic nanoparticles ($Fe_3O_4/SiO_2/NH_2/CHO$) with Fe_3O_4NPs' size of 30 nm (b) and Fe_3O_4NPs' size of 10 nm (c).

was found for the case of the synthesized Fe_3O_4NPs with a size of 10 nm.

For biological applications, GA was then added to the functionalized nanoparticles ($Fe_3O_4/SiO_2/NH_2$) to form the structure of $Fe_3O_4/SiO_2/NH_2/CHO$. As we mentioned above, protein A with an amount of 0.5 mg was mixed with the functionalized magnetic nanoparticles ($Fe_3O_4/SiO_2/NH_2/CHO$) with both sizes (10 nm and 30 nm). In this case, we expected that the smaller Fe_3O_4NPs offer higher binding efficiency than the bigger ones. It was due to the fact that the smaller nanoparticles have a large surface area/volume ratio [27]. This could be supported by the UV-Vis measurement of the absorption of protein A. Figure 6 shows the absorption spectrum of protein A for three cases including before immobilization on Fe_3O_4NPs (line a), after immobilization on Fe_3O_4NPs of 30 nm (line b), and after immobilization on Fe_3O_4NPs of 10 nm (line c). As expected, the absorbance at the peak of 280 nm, which was the standard peak for protein [47], decreased from 0.08 to 0.03 with the size of Fe_3O_4NPs changing from 30 nm to 10 nm, respectively. The binding efficiency (BE) can be calculated by the following equation:

$$\mathrm{BE}(\%) = \frac{C_{\mathrm{bd}}}{C_{\mathrm{tot}}}, \quad (2)$$

where C_{bd} is the concentration of protein A binding to Fe_3O_4NPs and C_{tot} is the initial concentration of protein A. Based on this measurement, we properly estimated the binding efficiency of protein A, which is 82% and 53% for size of the synthesized magnetic nanoparticles of 10 nm and 30 nm, respectively. To double-check the immobilization of protein on Fe_3O_4NPs, we conducted measurement using a fluorescent microscope. After immobilization of protein A on Fe_3O_4NPs, we added biotin-FITC on the solution. In this case, protein A can react with biotin-FITC through protein-protein interaction. As shown in Figure 7, the green color with a wavelength of 485 nm was emitted by FITC under excitation of the pump light. This indicated that biotin-FITC has been conjugated with protein A on the structure of $Fe_3O_4/SiO_2/NH_2/CHO$/protein A, leading to believe that protein A has been successfully immobilized.

The use of the synthesized magnetic nanoparticles may offer several benefits for drug delivery and detection of target proteins, as mentioned below. First, the silica layer can eliminate the toxicity of Fe_3O_4NPs when they are introduced into the human body for treatment. Additionally, the silica layer can also act as an insulating layer to control electron tunneling between particles, which may be important in charge transfer or magnetooptics. Second, surface modification via functional group immobilization is being pursued with great interest, since it can provide unique opportunities to engineer the interfacial of solid substrates while retaining particles' basic geometry. Moreover, the structure of $Fe_3O_4/SiO_2/NH_2/CHO$ can be conjugated with various proteins for specific target detection such as immunoglobulin G (IgG), which can specifically capture fibrinogen—a specific biomarker for heart disease and cardiovascular disease. Finally, the synthesized magnetic nanoparticles (10 nm) with magnetization of 85 emu/g can be used for drug delivery and cancer treatment by generation of heat under application of external magnetic field.

4. Conclusions

We presented the immobilization of protein A on the synthesized magnetic nanoparticles. The size of magnetic nanoparticles was controlled by the injection method of sodium hydroxide, leading to obtain the smaller size (10 nm) by immediate introduction of NaOH, due to the fact that the speed of sprout production was faster than the speed of crystal growth. The synthesized Fe_3O_4NPs with high magnetization of 85 emu/g offer benefits for drug delivery and cancer treatment. An immobilization of protein A on the functional

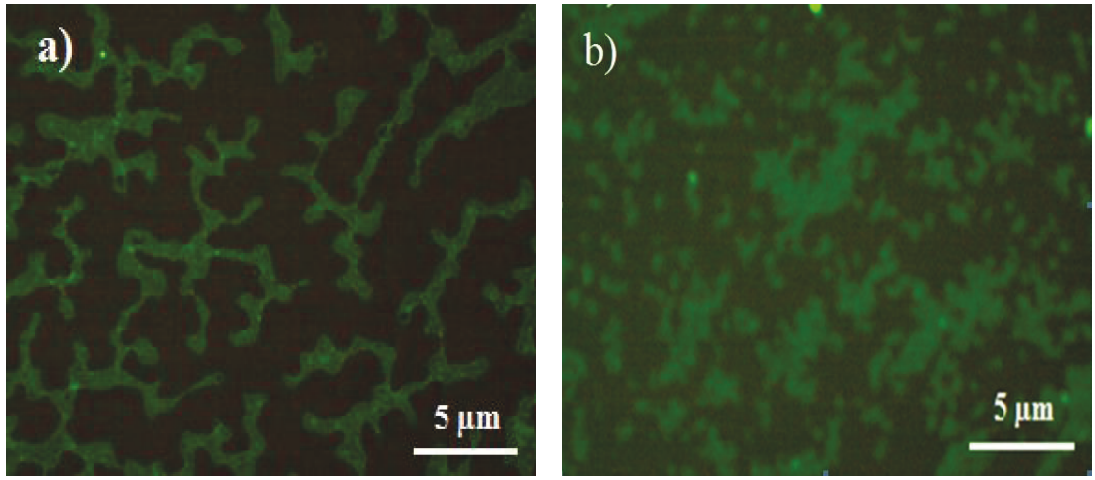

(a) (b)

Figure 7: Fluorescent microscope images of the structure of $Fe_3O_4/SiO_2/NH_2$/CHO/protein A after conjugation with biotin-FITC (a) size of 10 nm and (b) size of 30 nm.

Fe_3O_4NPs ($Fe_3O_4/SiO_2/NH_2$/CHO) with high efficiency of 82% presented may find potential applications for fibrinogen-based diagnosis of strokes, heart disease, cardiovascular disease, and Alzheimer's disease.

Data Availability

The data used to support the findings of this study are available from the corresponding author upon request.

Conflicts of Interest

The authors report no conflicts of interest in this work.

Acknowledgments

This research was supported by Tra Vinh University under Basic Science Research fund No. 607/HĐ.KHCN-ĐHTV.

References

[1] S. S. Morse, "Factors in the emergence of infectious diseases," in *Plagues and Politics*, Global Issues Series, A. T. Price-Smith, Ed., pp. 8–26, Palgrave Macmillan, London, 2001.

[2] N. P. A. S. Johnson and J. Mueller, "Updating the accounts: global mortality of the 1918-1920 "Spanish" influenza pandemic," *Bulletin of the History of Medicine*, vol. 76, no. 1, pp. 105–115, 2002.

[3] D. M. Morens, G. K. Folkers, and A. S. Fauci, "The challenge of emerging and re-emerging infectious diseases," *Nature*, vol. 430, no. 6996, pp. 242–249, 2004.

[4] B. Friguet, A. F. Chaffotte, L. Djavadi-Ohaniance, and M. E. Goldberg, "Measurements of the true affinity constant in solution of antigen-antibody complexes by enzyme-linked immunosorbent assay," *Journal of Immunological Methods*, vol. 77, no. 2, pp. 305–319, 1985.

[5] S. Lai, S. Wang, J. Luo, L. J. Lee, S. T. Yang, and M. J. Madou, "Design of a compact disk-like microfluidic platform for enzyme-linked immunosorbent assay," *Analytical Chemistry*, vol. 76, no. 7, pp. 1832–1837, 2004.

[6] S. S. An, T. T. Nguyen, S. O. Bae et al., "A regenerative label-free fiber optic sensor using surface plasmon resonance for clinical diagnosis of fibrinogen," *International Journal of Nanomedicine*, vol. 10, pp. 155–163, 2015.

[7] J. S. Lee, "Alternative dideoxy sequencing of double-stranded DNA by cyclic reactions using *Taq* polymerase," *DNA and Cell Biology*, vol. 10, no. 1, pp. 67–73, 1991.

[8] C. G. Koh, W. Tan, M. Q. Zhao, A. J. Ricco, and Z. H. Fan, "Integrating polymerase chain reaction, valving, and electrophoresis in a plastic device for bacterial detection," *Analytical Chemistry*, vol. 75, no. 17, pp. 4591–4598, 2003.

[9] M. Kubista, J. M. Andrade, M. Bengtsson et al., "The real-time polymerase chain reaction," *Molecular Aspects of Medicine*, vol. 27, no. 2-3, pp. 95–125, 2006.

[10] T. T. Nguyen, K. T. L. Trinh, W. J. Yoon, N. Y. Lee, and H. Ju, "Integration of a microfluidic polymerase chain reaction device and surface plasmon resonance fiber sensor into an inline all-in-one platform for pathogenic bacteria detection," *Sensors and Actuators B: Chemical*, vol. 242, pp. 1–8, 2017.

[11] V. J. Mohanraj and Y. Chen, "Nanoparticles-a review," *Tropical Journal of Pharmaceutical Research*, vol. 5, no. 1, pp. 561–573, 2006.

[12] E. Royston, A. Ghosh, P. Kofinas, M. T. Harris, and J. N. Culver, "Self-assembly of virus-structured high surface area nanomaterials and their application as battery electrodes," *Langmuir*, vol. 24, no. 3, pp. 906–912, 2008.

[13] X. Chen and C. Burda, "The electronic origin of the visible-light absorption properties of C-, N- and S-doped Tio_2 nanomaterials," *Journal of the American Chemical Society*, vol. 130, no. 15, pp. 5018-5019, 2008.

[14] Z. Y. Zhou, N. Tian, J. T. Li, I. Broadwell, and S. G. Sun, "Nanomaterials of high surface energy with exceptional properties in catalysis and energy storage," *Chemical Society Reviews*, vol. 40, no. 7, pp. 4167–4185, 2011.

[15] Z. Liu, A. . C. Fan, K. Rakhra et al., "Supramolecular stacking of doxorubicin on carbon nanotubes for in vivo cancer therapy," *Angewandte Chemie International Edition*, vol. 48, no. 41, pp. 7668–7672, 2009.

[16] S. R. Ji, C. Liu, B. Zhang et al., "Carbon nanotubes in cancer diagnosis and therapy," *Biochimica et Biophysica Acta (BBA) - Reviews on Cancer*, vol. 1806, no. 1, pp. 29–35, 2010.

[17] L. Wang, W. Zhao, and W. Tan, "Bioconjugated silica nanoparticles: development and applications," *Nano Research*, vol. 1, no. 2, pp. 99–115, 2008.

[18] C. Argyo, V. Weiss, C. Bräuchle, and T. Bein, "Multifunctional mesoporous silica nanoparticles as a universal platform for drug delivery," *Chemistry of Materials*, vol. 26, no. 1, pp. 435–451, 2013.

[19] J. G. Croissant, Y. Fatieiev, A. Almalik, and N. M. Khashab, "Mesoporous silica and organosilica nanoparticles: physical chemistry, biosafety, delivery strategies, and biomedical applications," *Advanced Healthcare Materials*, vol. 7, no. 4, p. 1700831, 2018.

[20] B. Rühle, P. Saint-Cricq, and J. I. Zink, "Externally controlled nanomachines on mesoporous silica nanoparticles for biomedical applications," *ChemPhysChem*, vol. 17, no. 12, pp. 1769–1779, 2016.

[21] S. Shrivastava, T. Bera, A. Roy, G. Singh, P. Ramachandrarao, and D. Dash, "Characterization of enhanced antibacterial effects of novel silver nanoparticles," *Nanotechnology*, vol. 18, no. 22, article 225103, 2007.

[22] V. Gopinath, D. MubarakAli, S. Priyadarshini, N. M. Priyadharsshini, N. Thajuddin, and P. Velusamy, "Biosynthesis of silver nanoparticles from *Tribulus terrestris* and its antimicrobial activity: a novel biological approach," *Colloids and Surfaces B: Biointerfaces*, vol. 96, pp. 69–74, 2012.

[23] R. Elghanian, J. J. Storhoff, R. C. Mucic, R. L. Letsinger, and C. A. Mirkin, "Selective colorimetric detection of polynucleotides based on the distance-dependent optical properties of gold nanoparticles," *Science*, vol. 277, no. 5329, pp. 1078–1081, 1997.

[24] J. Liu and Y. Lu, "A colorimetric lead biosensor using DNAzyme-directed assembly of gold nanoparticles," *Journal of the American Chemical Society*, vol. 125, no. 22, pp. 6642-6643, 2003.

[25] S. Ogawa, T. M. Lee, A. R. Kay, and D. W. Tank, "Brain magnetic resonance imaging with contrast dependent on blood oxygenation," *Proceedings of the National Academy of Sciences of the United States of America*, vol. 87, no. 24, pp. 9868–9872, 1990.

[26] P. Marckmann, L. Skov, K. Rossen et al., "Nephrogenic systemic fibrosis: suspected causative role of gadodiamide used for contrast-enhanced magnetic resonance imaging," *Journal of the American Society of Nephrology*, vol. 17, no. 9, pp. 2359–2362, 2006.

[27] A. K. Gupta and M. Gupta, "Synthesis and surface engineering of iron oxide nanoparticles for biomedical applications," *Biomaterials*, vol. 26, no. 18, pp. 3995–4021, 2005.

[28] R. Hao, R. Xing, Z. Xu, Y. Hou, S. Gao, and S. Sun, "Synthesis, functionalization, and biomedical applications of multifunctional magnetic nanoparticles," *Advanced Materials*, vol. 22, no. 25, pp. 2729–2742, 2010.

[29] C. Xu and S. Sun, "New forms of superparamagnetic nanoparticles for biomedical applications," *Advanced Drug Delivery Reviews*, vol. 65, no. 5, pp. 732–743, 2013.

[30] C. Xu and S. Sun, "Monodisperse magnetic nanoparticles for biomedical applications," *Polymer International*, vol. 56, no. 7, pp. 821–826, 2007.

[31] M. Longmire, P. L. Choyke, and H. Kobayashi, "Clearance properties of nano-sized particles and molecules as imaging agents: considerations and caveats," *Nanomedicine*, vol. 3, no. 5, pp. 703–717, 2008.

[32] C. Pisani, J. C. Gaillard, M. Odorico et al., "The timeline of corona formation around silica nanocarriers highlights the role of the protein interactome," *Nanoscale*, vol. 9, no. 5, pp. 1840–1851, 2017.

[33] S. Dib, M. Boufatit, S. Chelouaou et al., "Versatile heavy metals removal *via* magnetic mesoporous nanocontainers," *RSC Advances*, vol. 4, no. 47, pp. 24838–24841, 2014.

[34] M. Z. Iqbal, X. Ma, T. Chen et al., "Silica-coated superparamagnetic iron oxide nanoparticles (SPIONPs): a new type contrast agent of T_1 magnetic resonance imaging (MRI)," *Journal of Materials Chemistry B*, vol. 3, no. 26, pp. 5172–5181, 2015.

[35] W. Koenig, M. Sund, M. Fröhlich et al., "C-reactive protein, a sensitive marker of inflammation, predicts future risk of coronary heart disease in initially healthy middle-aged men," *Circulation*, vol. 99, no. 2, pp. 237–242, 1999.

[36] R. Massart, "Preparation of aqueous magnetic liquids in alkaline and acidic media," *IEEE Transactions on Magnetics*, vol. 17, no. 2, pp. 1247-1248, 1981.

[37] M. C. Mascolo, Y. Pei, and T. A. Ring, "Room temperature co-precipitation synthesis of magnetite nanoparticles in a large pH window with different bases," *Materials*, vol. 6, no. 12, pp. 5549–5567, 2013.

[38] J. Zhao, M. Milanova, M. M. C. G. Warmoeskerken, and V. Dutschk, "Surface modification of TiO_2 nanoparticles with silane coupling agents," *Colloids and Surfaces A: Physicochemical and Engineering Aspects*, vol. 413, pp. 273–279, 2012.

[39] K. Can, M. Ozmen, and M. Ersoz, "Immobilization of albumin on aminosilane modified superparamagnetic magnetite nanoparticles and its characterization," *Colloids and Surfaces B: Biointerfaces*, vol. 71, no. 1, pp. 154–159, 2009.

[40] S. Minko, "Grafting on solid surfaces: "grafting to" and "grafting from" methods," in *Polymer Surfaces and Interfaces*, M. Stamm, Ed., pp. 215–234, Springer, Berlin, Heidelberg, 2008.

[41] B. D. Cullity and J. W. Weymouth, "Elements of X-ray diffraction," *American Journal of Physics*, vol. 25, no. 6, pp. 394-395, 1957.

[42] Y. Liu, S. Jia, Q. Wu, J. Ran, W. Zhang, and S. Wu, "Studies of Fe_3O_4-chitosan nanoparticles prepared by co-precipitation under the magnetic field for lipase immobilization," *Catalysis Communications*, vol. 12, no. 8, pp. 717–720, 2011.

[43] J. P. Abid, A. W. Wark, P. F. Brevet, and H. H. Girault, "Preparation of silver nanoparticles in solution from a silver salt by laser irradiation," *Chemical Communications*, vol. 7, no. 7, pp. 792-793, 2002.

[44] D. Kim, S. Jeong, and J. Moon, "Synthesis of silver nanoparticles using the polyol process and the influence of precursor injection," *Nanotechnology*, vol. 17, no. 16, pp. 4019–4024, 2006.

[45] J. Zou, Y. G. Peng, and Y. Y. Tang, "A facile bi-phase synthesis of Fe_3O_4@SiO_2 core–shell nanoparticles with tunable film thicknesses," *RSC Advances*, vol. 4, no. 19, pp. 9693–9700, 2014.

[46] M. Klotz, A. Ayral, C. Guizard, C. Ménager, and V. Cabuil, "Silica coating on colloidal maghemite particles," *Journal of Colloid and Interface Science*, vol. 220, no. 2, pp. 357–361, 1999.

[47] W. H. Habig, M. J. Pabst, and W. B. Jakoby, "Glutathione S-transferases: the first enzymatic step in mercapturic acid formation," *Journal of Biological Chemistry*, vol. 249, no. 22, pp. 7130–7139, 1974.